
Article:
Bowman, E. orcid.org/0000-0001-7868-6688 and Hunter, R.P. (2018) Visualisation of seepage induced suffusion and suffosion within internally erodible granular media. Géotechnique, 68 (10). pp. 918-930. ISSN 0016-8505

https://doi.org/10.1680/jgeot.17.P.161

Visualisation of seepage induced suffusion and suffosion within internally erodible granular media

R.P. Hunter, E.T. Bowman

ABSTRACT

A rigid walled ‘transparent soil’ permeameter has been developed to visually study the mechanisms occurring during seepage induced internal erosion in susceptible granular media under upward flow. The experiments use borosilicate glass particles in place of soil, and an optically matched oil mixed with fluorescent dye in place of water. The technique known as Plane Laser Induced Fluorescence (PLIF) enables a two-dimensional plane of particles and fluid to be viewed inside the permeameter, away from the walls. Results of tests have provided close agreement with those of other researchers on soil of comparable particle size grading. Unstable materials showed migration of fine grains under mean hydraulic gradients as low as i = 0.25, while stable materials eventually failed by heave at hydraulic gradients close to unity. Internally unstable soils where the loads were predominantly supported by the coarser fraction exhibited suffusion (fines migration without disruption of the load bearing system); those supported by both coarse and fine particles exhibited suffosion (i.e. volume change during fines migration). Quantitative image analysis conducted on one unstable sample showed areas of open void space migrating though the sample at low hydraulic gradients near critical, as defined by Skempton and Brogan (1994). This occurred before the externally measured local hydraulic gradients began to significantly diverge from the mean. The testing technique developed shows that optically matched glass and oil behave mechanically similarly to soil and water, and that the PLIF technique coupled with image analysis can provide additional insight to the mechanisms of internal erosion.

NOTATION

C_u	uniformity coefficient = (D_{60}/D_{10})
D	grain size (mm)
$(D'_{15}/d'_{85})_{max}$	maximum grain size ratio between coarser fraction and finer fraction, after the PSD has been split, following the Kezdi (1979) analysis
$(D'_{15}/d'_{85})_{min}$	minimum grain size ratio between coarser fraction and finer fraction, after the PSD has been split, following the Kezdi (1979) analysis
D'_{15}	grain size of the coarser fraction where 15% by weight is finer (mm)
d'_{85}	grain size of the finer fraction where 85% by weight is finer (mm)
D_{10}	particle size for which 10% of the soil is finer (cm)
D_{eff}	effective diameter
e	void ratio
F	mass fraction smaller than particle diameter, D
g	gravitational acceleration ($m.s^{-2}$)
H	a particle size between D and 4D
i	hydraulic gradient
i_{av}	average hydraulic gradient
i_c	theoretical critical hydraulic gradient
i_{cr}	critical hydraulic gradient observed in test
k	Darcy's permeability ($m.s^{-1}$)
n	porosity
PSD	particle size distribution
t	time elapsed (s)
v	velocity (ms^{-1})
σ_{v0}	applied vertical effective stress
σ_{vm}	mean vertical effective stress
α	'alpha' reduction factor
σ'_f	effective stress of finer particles
ρ	specific gravity
γ	unit weight of permeant
γ'	average effective stress
γ'_z	average effective stress across a section at depth, z
γ_w	unit weight of water

1 INTRODUCTION

Internal erosion of susceptible granular materials under fluid flow can affect the performance of geotechnical structures designed to control seepage, such as cut off walls, dams and levees. Particle size distribution, seepage hydraulic gradient and mean stress are all known to be factors influencing the occurrence of internal erosion, however many questions remain as to how it is locally manifested, and how suffusion of fines through a matrix of coarse particles can lead to structure collapse and eventual settlement, in a process sometimes called suffosion (Moffat et al, 2011; Fannin and Slangen, 2014).

Previous experimental studies to visually examine the mechanisms of internal erosion include those by Rosenbrand and Dijkstra (2012) and Ouyang and Takahashi (2015). These studies focused on the use of image analysis to examine particle movement at the sidewalls of a test sample undergoing internal erosion. Here we describe a new transparent soil permeameter, designed to enable two dimensional planes within a granular material matrix to be observed away from the influence of the apparatus side walls. In this way, the particle structure or fabric and the movement of individual particles under seepage can be directly viewed and hence, the internal erosion process examined in detail. The technique uses glass particles and a fluid whose combined physical and optical properties have been carefully selected to replicate soil-fluid interaction, but with added advantage of optical transparency (Matsushima et al., 2002; Sanvitale and Bowman, 2012). The use of Plane Laser Induced Fluorescence, PLIF, further enables examination of the initial and changing particle fabric of a selected two-dimensional plane within the granular system, under increasing rates of seepage. We present the experimental results of tests on particle size distributions that have been chosen to replicate, as far as possible, those from two previous studies, Skempton and

Brogan (1994) and Fannin and Moffat (2006). The results show that angular glass is capable of replicating behaviour of real soil under seepage, and highlight that internal erosion is a localized process, even within a relatively small granular element. The results also lend further support to the use of stability criteria as proposed by Kenney and Lau (1985) for the assessment of internal stability of soils.

2 METHOD

2.1 Experimental arrangement

The experimental design uses a rigid wall permeameter that is intended to replicate that designed by Skempton and Brogan (1994), but with the enhanced capability of being able to view particles beyond the external boundaries as they are internally eroded. The solid fraction consists of a particle size distribution of transparent granular solids that are adjudged to be internally stable or unstable, according to the stability criteria proposed by Kenney and Lau (1985). Refractively matched immersion oil (Cargille Labs) with a small amount of fluorescent Rhodamine dye added is used as the permeant in upward flow. The method uses PLIF via refractive index matching of the solids and fluid, and a thin laser sheet applied to the materials through the sidewalls of the permeameter. As the hydraulic gradient of the test is increased in a stepwise manner, digital images of the illuminated plane of particles of interest are recorded and compared with the seepage velocity and local hydraulic gradient, until local piping failure or heave occurs.

2.2 Test materials

Table 1 shows relevant physical and optical properties of the solids and fluid which were required to be optically matched, non-toxic and exhibit a difference in density comparable to

that of soil and water. In this case the density ratio was 2.65:1, i.e. the same as quartz to water.

The irregular shape of natural soil particles is important to soil behaviour and to internal erosion in particular, with irregular particles producing more options for packing than spherical particles and more tortuous flow paths (Marot et al. 2012). Therefore in order for the glass particles to replicate soil as closely as possible, in these experiments irregular particles were manufactured from breaking rods and tubes of borosilicate glass, in a similar manner to that detailed by Sanvitale and Bowman (2012). Larger cut particles were sub-angular to sub-rounded in shape while smaller crushed particles were more angular, with most particles having low surface roughness, associated with the smooth nature of glass.

2.3 Apparatus and sample preparation

The internal dimensions of the permeameter were: 100mm by 100mm in plan area and 265mm in height (Figure 1). Five manometer ports, denoted p1 to p5, were arranged as a vertical array at the back of the permeameter for local head measurement, leaving the front and sides clear for the application of the laser technique. A header tank above the apparatus was used to generate the flow of oil upward through the permeameter that exited via outlet pipes at the top into a holding tank (Figure 2). In order to dissipate the flow entering the permeameter so that an even flow traveled into the filter sample, a 50 mm layer of 'dispersing' filter material was placed at the bottom of the apparatus. This material was selected so that it was between four times the 15% size ($4D_{15}$) and four times the 85% size ($4D_{85}$) of the sample being tested. Once this material was placed, the oil control valves were opened, allowing oil to permeate to the top of the dispersing filter, before the valves were closed. A thin glass rod was used to stir air bubbles out of the oil, before a steel frame and gauze were placed over the dispersing filter, ready for the filter sample to be placed on top.

A specific particle size distribution (PSD) for testing would be created be weighing out the appropriate proportions of each size, using British Standard sieve sizes, evenly across four separate containers. Then immersion oil was poured into the bowls and gently stirred. The bowls were then placed into a vacuum desiccator for 2-3 hours to de-air the sample. Gentle stirring was required to release remaining air bubbles upon removal from the vacuum. The sample was then ready for placement into the permeameter. A variety of sample placement methods was trialled, with the 'slurry' technique proving most reproducible. The particles were gently stirred to generate an even distribution of particle sizes, and then using a teaspoon with the head bent at 90°, particles were scooped out and gently placed into the upper screen within the apparatus. Oil had been allowed into the apparatus so that the upper screen was just immersed with oil, in an attempt to keep the sample saturated while being placed. This method gave a 'loose' compaction, and care was taken not compact any part of the sample to ensure repeatability.

2.4 Testing procedure

During testing, a calibrated rotameter between the header tank and permeameter enabled the flow rate to be measured at any point in time, while the flowrate was also directly measured periodically by intercepting fluid returning to the holding tank. A pump was used to recirculate the oil into the header tank, thus conserving it throughout the experiments, which generally lasted several hours.

To enable viewing inside the prepared sample, a 1.5 mm wide 532nm plane laser sheet was applied at one side (right in Figure 2), normal to the side face with viewing from the front. The laser could be placed at any distance from the front viewing plane, but was generally held within the front 15mm where clarity was best. Upon each increment in head being applied, images were taken using a high speed camera (MotionPro Y4-S1) set at a relatively low rate to capture the movements of particles within the plane of interest.

Each increment in head (initially of 2 cm, reducing to 1 cm as local movement of fine particles began) was applied for a period of approximately 20 minutes which was sufficient to ensure that no further movement of particles or other changes could be detected either visually or via the manometer readings. The camera, generally at an acquisition rate of 10 frames per second, with a long pass filter to limit imaging to the emission wavelength of the fluorescent dye, was placed perpendicular to and focused upon the illuminated plane. Figure 2 shows a typical experimental arrangement for a given test; further details may be found in Hunter (2012).

2.5 Tests conducted

This paper discusses the behaviour of three test materials that were designed to replicate those of Skempton and Brogan's (1994) "Sample A", "Sample B" and "Sample D" (denoted GS&B-A, GS&B-B and GS&B-D). In addition, one sample from Fannin and Moffat (2006), G4-C* (G-G4-C), was also replicated and one sample, with a PSD intermediate to Skempton and Brogan's Samples A and B, was tested (GS&B-H). Sample A was defined by Skempton and Brogan as being unstable with respect to internal erosion, while Sample B was just unstable and sample D was stable. In these cases, load was considered to be supported via the coarser fraction according to an assessment of the fines content. In contrast, in Fannin and Moffat (2006), G4-C* was considered unstable with load being carried by a matrix of both coarse and fine particles (Shire and Sullivan, 2013).

With respect to the replicates created in this study, as a result of the fluid viscosity being higher than that of water (Table 1), the overall permeability of the system would be lower than if water were used for the same PSD. Sanvitale and Bowman (2012) used fluid-particle scaling to determine that for these materials, the PSD needed to be scaled up in size by $\sqrt{20}$ or approximately 4.4 times to counter the decrease in permeability. Increasing particle size has

the benefit that particles are easier to see, however it also leads to greater arching across the rigid walls than if the particles were smaller. Hence here, particle size distributions for Skempton and Brogan's Samples A and B as well as Fannin and Moffat's G4-C* were increased by four times, where fine particle migration may be expected, and for two times for D, where the sample should heave at failure. In addition, to reduce arching without altering the particle-fluid interactions appreciably, the very uppermost part of the scaled PSDs for the Skempton and Brogan replicates were removed, so that those above were replaced by particles of 19mm for GS&B-A, GS&B-B a and 9.5mm for GS&B-D. No change in the shape of the PSD for the G4-C* replicate was made. The resultant glass test PSDs with particles replaced as described are shown in Figure 3 as "GS&B-A", "GS&B-B" and "GS&B-D" against the original ones used by Skempton and Brogan (1994) and "G-G4-C" against the original material tested by Fannin and Moffat (2006). GS&B-H is a stand alone test in terms of PSD, however, close up photography was used for this test in order to examine the possibility of using image analysis to quantify erosion.

3 INTERNAL STABILITY

3.1 Critical Hydraulic Gradient

Terzaghi (1925) defined the critical upward hydraulic gradient i_c for sands as:

$$i_c = (1 - n)(1 - \rho) = \frac{(\gamma - \gamma_w)}{\gamma_w} = \frac{\gamma'}{\gamma_w} \qquad (1)$$

Where n is the porosity of the material, ρ is the specific gravity of the grains, γ is the bulk unit weight of the material (solids and fluid), γ_w is the unit weight of fluid and γ' is the buoyant unit weight. This equation suggests that the critical gradient should occur when the overburden stress of the grains is equal to the upward flow stress from the fluid.

In Terzaghi's equation (1), the permeant is usually water and the specific gravity is therefore determined relative to water (i.e. ρ of 2.65 for quartz grains assumes a value of unity for water). Here, both solid particles and fluid are less dense than quartz and water, respectively. The specific gravity ρ here should therefore be the ratio of glass to oil (from Table 1), i.e. 2230 / 846 = 2.636, which happens to be close to typical values for soil compared with water. Hence, i_c is determined from the reported porosities and ρ of 2.636.

Skempton and Brogan (1994) found that in their internally unstable tests, Darcian flow occurred until a critical hydraulic gradient i_{cr} was reached, whereupon fines began to migrate within the sample. The value for i_{cr} was found to be significantly lower than that calculated using Equation 1. The authors proposed that the most likely reason for this was that the overburden load was being predominantly carried by the coarser fraction, a notion supported by recent numerical work (Shire et al., 2014). They proposed that where the fine grains initially carry some proportion of the overburden load, then the effective stress on the finer particles (σ_f'), which is only a portion of the effective stress on the coarser particles (σ'), can be described by:

$$\sigma_f' = \alpha \gamma' z \qquad (2)$$

Where α is a reduction factor and $\gamma' z$ is the average effective stress across a section at depth z, which is also σ'. Therefore, the critical gradient for piping in the fine grains will be:

$$i_{cr} = \alpha \left(\frac{\gamma'}{\gamma_w}\right) \text{ or } i_{cr} = \alpha i_c \qquad (3)$$

Where i_{cr} is the critical hydraulic gradient observed in the test. This relationship describes that a larger α will yield a greater resistance to the onset of seepage-induced instability, as outlined by Li and Fannin (2012).

3.2 Internal stability assessments

Various criteria for internal stability have been proposed, based on analyses of the particle size distribution, PSD. Some of the most commonly used are those based on Kenney and Lau (1985), Istomina (1957), Kezdi (1979), Burenkova (1993), and Wan and Fell's (2008) modified (probabilistic) Burenkova method for gap-graded soils. These criteria were used here, to attempt to predict the propensity for the samples used in these tests to internally erode as given in Table 2.

3.3 Image quality and degradation

Figure 4 shows plane laser images taken at depths of 10 mm, 20 mm, and 30 mm from the front of the box for a typical test. With increasing depth through the sample, minor mismatches in refractive index, impurities and air bubbles cause a reduction in clarity. Images for the tests described were taken at a depth of approximately 15 mm from the front of the transparent box. This was deemed to be sufficiently far from the front to be representative of the whole, while maintaining excellent optical sharpness. Hydraulic gradient was measured at the back of the sample.

3.4 Flow velocity versus hydraulic gradient & microstructural change

The average hydraulic gradient against flow velocity for each test are presented in Figure 5 to 12 for the four tests in addition to internal images taken before and during the tests. For GS&B-B, a sequence of images is also presented in parallel with the hydraulic gradient

observations (noting that the equivalent for GS&B-A is presented in Hunter and Bowman, (2015)). In a similar vein to Skempton and Brogan (1994), we discuss the behaviour of the tests with reference to these figures.

3.4.1 GS&B-A

With reference to Figure 5 (hydraulic gradient versus flow velocity) and Figure 6 (image planes taken (a) before the application of seepage and (b) during piping), the following stages of development were observed:

a) At i_{av} = 0.153 there was a slight movement of fines in void spaces, both along the glass edges and within the sample upon first increasing the flow rate. Particles stabilised after approximately 30 seconds. The permeability was constant at k = 0.30 cm/s until i_{av} = 0.23.
b) At i_{av} = 0.23 there was a break in Darcian flow, with an increase in i_{av} versus flow velocity.
c) From i_{av} = 0.248 to 0.286, fines began to slowly move upwards through the sample, and 'dancing-like' movements were seen in some voids. At i_{av} = 0.276, k = 1.6 cm/s.
d) At i_{av} = 0.286 strong general piping, or suffusion, initiated throughout the sample and fines migrated up through the sample, while larger gravel-sized particles remained undisturbed. There was an increase in flow velocity gradient marking an increased permeability k = 3.3 cm/s.
e) Up to i_{av} = 0.381 strong general piping continued without 'violent piping' being observed (Skempton & Brogan, 1994). Compare Figure 6 (b) with (a) which shows the movement of fines but no change in the clast supported structure.

The critical hydraulic gradient due to piping for GS&B-A was determined as i_{cr} = 0.248, giving α = 0.21. A supplementary image sequence taken during local pipe formation with

suffusive behaviour for an additional test on this material is provided at S1 (Supplementary material S1).

3.4.2 GS&B-B

For sample GS&B-B, which was considered to be marginally stable according to Kenney and Lau (1985), observations of the images are given in detail here, in addition to a commentary on the overall behaviour in terms of flow velocity and hydraulic gradient. The following was observed (see Figure 7 in conjunction with Figure 8).

a) From i_{av} = 0.10 to 0.16 there was a slight movement of fine particles in some void spaces of the sample. The permeability was k = 1.0 cm/s.

b) From i_{av} = 0.23 to 0.50 there was an increase in gradient between i_{av} and v. At i_{av} = 0.23 there was an increase in the number of fine particles moving in localised void spaces. At i_{av} = 0.30 a slight migration of fines initiated throughout voids in the sample, which increased at i_{av} = 0.39. The permeability during this time was k = 1.46 cm/s.

c) At i_{av} = 0.50 some of the coarser fraction made small readjustments in their structure, inside void areas. Finer particles also continued to move. These movements only occurred where void spaces were present, however. In parts of the sample where there were few voids there was no noticeable particle movement, and these sections appeared stable.

d) At i_{av} = 0.62 to 0.88 the flow velocity became high, resulting in the oil becoming aerated due to limitations in the equipment, which resulted in decreased image quality. At this hydraulic gradient, there was a continued movement of the some of the coarser fraction while fine fraction also continued to migrate upwards where possible. The permeability reduced to k = 0.72 cm/s, possibly due to the intrusion of

air bubbles, although there may also have been some restabilization of the particle fabric.

e) At i_{av} = 1.01 the sample heaved.

Both fabric observation and flow rate / hydraulic gradient observation suggest meta-stability. That is, the sample appeared to develop fines migration behaviour associated with internal erosion at i_{cr} = 0.3, which results in a calculated alpha value of α = 0.26, however, the overall fabric was somewhat stable, enabling the hydraulic gradient to be increased until heave failure at α = 0.87. We consider the sample to be just unstable, considering that the degree of fines migration would be unacceptable under field conditions, and over longer time might result in further collapse.

3.4.3 GS&B-D

For the test on Sample GS&B-D, the flow rate values are estimated based on calibrated rotameter data (Figure 9). Due to smaller particles being used overall compared with GS&B-A and GS&B-B (Figure 10), the initial permeability was lower. The theoretical critical hydraulic gradient at heave was i_c = 1.162.

The following observations were made during the test:

a) From commencement of flow until i_{av} = 1.16, there were small translational and/or rotational movements of some of the finer grains in void spaces, generally underlying larger grains, where the upward flow pressed smaller grains into the overlying larger grains. The specimen appeared stable up to this point. During this time the permeability k = 0.18 cm/s. This can be compared with 1.0 cm/s for GS&B-B, which for the same reduced scaling would have an equivalent k of approximately 0.25 cm/s (i.e. four times lower than determined). Hence the data are in line with expectations.

b) Upon the next head rise to i_{av} = 1.31, the entire sample experienced an upward translation, or heave, of approximately 1 mm. The permeability during this time was k = 0.25 cm/s (Figure 10).

c) Until i_{av} = 1.63, each subsequent raise in head lifted the entire specimen slightly higher. At this hydraulic gradient it rose to an additional height of 6.8 mm whereupon particles fell from the base of the sample as turbulent flow under the sample initiated.

Using a critical hydraulic gradient, i_{cr} = 1.31, yields α = 1.13, which suggests there may have been some additional stability gained from sidewall rigidity – i.e. arching. Alternatively, as Figure 9 shows, extrapolating back the flow velocity during heave to the behaviour before heave results in an intercept of around i = 1.2, which would give α = 1.03, suggesting that a smaller head increment may have led to a closer result to the theoretical value.

3.4.4 G-G4-C

This test case examines the influence of the degree of fill of the voids by fines on the behaviour of the whole under increasing seepage flow. In the tests by Skempton and Brogan (1994) and its replicates here in glass, the voids were underfilled, with an approximate percentage by mass of fines of 15%. This is considerably lower than the theoretical minimum fill limit of 24-29% below which small grains sit within the voids of the larger grains, i.e. are clast supported (Skempton and Brogan, 1994). Conversely, Fannin and Moffat (2006) tested an idealised gap graded PSD, which they termed G4-C*, in which the soil fines filled the voids at 40% by mass. This is above the maximum limit of 35% determined by Skempton and Brogan (1994) above which larger grains are theoretically completely surrounded by fines. The test described here directly replicates this test with upscaled angular glass particles. Results are presented in Figures 11 and 12, and a supplementary video is provided

at S2 (Supplementary material S2), showing the structure collapse downwards as the fines migrate (note that the fines appear to move down, but in fact are moving up in the sequence).

Observations from the test:

a) From i_{av} = 0 to i_{av} = 0.40 no movement of particles was observed. The permeability was constant at k = 0.02 cm/s (Figure 11).
b) At i_{av} = 0.5 there was a small movement of some fines which moved into small voids, typically between two larger particles
c) From i_{av} = 0.58 to i_{av} = 0.72 fines near the top of the sample began to move along the glass edges. There was a very slight increase in sample height as fines began to deposit at the top of the specimen (Figure 12).
d) Upon the next raise in head of 1 cm, the sample suddenly failed by piping in the front left corner. In watching the sequence of images in succession (supplementary video at S2 shows 100 frames over ten seconds), the fines can be seen washing out of the sample, resulting in the collapse of the coarser particle structure as the fines are removed (i.e. 'suffosion' as defined by Fannin and Slangen (2014)). In the video, as failure is seen to initiate on the left side, the collapse first occurs on this side, but as the wash out of fines progresses over to the right side, it too collapses down. The fines are deposited at the top of the specimen in a mound.

Given the critical hydraulic gradient i_{cr} = 0.72, the alpha value was found to be 0.798.

3.4.5 GS&B-H

For this final test, a calibration dot target was set at various depths within the apparatus, prior to the placement of the glass material. The dots spaced at known distances allowed a scale to

be added to the images, which was used for scaling during image processing, as discussed later in Section 6. During the test, the following was observed. :

a) From i_{av} = 0 to i_{av} = 0.152 permeability was constant at k = 0.50 cm/s. Small movements of fines were observed along the glass walls from i_{av} = 0.057.
b) From i_{av} = 0.15 to i_{av} = 0.19 fines began to suffuse through the coarser clasts, leaving new void spaces within the material. This occurred throughout all parts of the sample, although the mean and local hydraulic gradient values, i_{12}, i_{23}, i_{34}, between manometer ports p1, p2, p3 and p4 (Figure 1) remained similar.
c) At i_{av} = 0.19 there was an increase in average permeability to k = 1.17 cm/s while the local hydraulic gradients, i_{12}, i_{23}, i_{34}, began to diverge from the average, i_{av}. Fines continued to move throughout the sample, with some of the smaller, coarse grains making minor movements.
d) At i_{av} = 0.33 piping along the centre, front edge of the permeameter initiated, and a mound of fines began accumulating at the surface. Some of the smaller coarse fraction moved in void spaces as fines were washed from the specimen. The overall permeability increased to k = 1.47 cm/s and remained approximately constant until i_{av} = 0.48. The test was terminated at i_{av} = 0.6. During this period, the local hydraulic gradients diverged significantly from the mean.

The critical hydraulic gradient in the test, i_{cr} = 0.15 leads to an alpha value of α = 0.128.

4 REPLICATION ANALYSIS

In order to determine whether the glass-oil mixtures can be considered a good analogue for soil and water, Table 3 compares the data from the tests described with those that they were designed to replicate.

4.1 Grading extremes

At the two extremes of grading stability, agreement between results of tests on Skempton and Brogan's (1994) Sample A, S&B-A (piping at α = 0.18) and GS&B-A (piping at α = 0.21) and that of Sample D, S&B-D (heave at α = 0.95) and GS&B-D (heave at α = 1.13, or earlier) is excellent. To put into further context, for highly gap graded samples similar to Sample A, Li (2008) found α of 0.13 for a larger specimen, while Shire et al. (2014) found α to range between 0.04 and 0.15 from dense to loose samples in numerical simulations on similarly under-filled fabrics.

4.2 Intermediate gradings

For the intermediate graded specimens the picture is a little more complex. The glass GS&B-B specimen had a somewhat higher initial permeability than Skempton and Brogan's Sample B (S&B-B). This then increased as fines were washed out of the material and general movement of fines began at i_{av} = 0.3, resulting in α = 0.26 (compared with 0.34 for S&B-B). However, at i_{av} = 0.5 the permeability reduced from k = 1.46 cm/s to k = 0.72 cm/s, which coincided with a rearrangement of some coarser particles, and with aeration of the oil. The restabilized system finally failed by heave. It's not known exactly how much of the reduction in permeability was caused by oil aeration compared to the structural rearrangement, but a clue as to the importance of the air entrainment can be gained from examining the final α value at heave which was determined as 0.85. If it is assumed that the "true" α value for heave must be approximately unity (and any arching would result in higher values again, as

with GS&B-D), this would suggest that i_c used in the calculation of α here is too high. That is, air bubbles may be considered as weightless particles, which would reduce the mean solid mass in comparison to the fluid, resulting in premature heave failure in comparison with a calculation based on the specific gravity of the particles alone. However, irrespective of the actual α value, it is clear that sample GS&B-B was a metastable material – and might have failed either by heave or piping under a slightly different packing.

Regarding the final test comparison, Fannin and Moffat's (2006) G4-C* sample had 25kPa stress applied at the top, while no additional stress was applied in the test described here. In Li and Fannin (2012), a hydromechanical envelope is presented which expands on the alpha factor to include the influence of effective stress as well as upward flow stress. Their formula that defines the hydromechanical envelope for heave of an internally stable soil is given by:

$$i_{\gamma c} = \frac{\sigma_{v0}}{\gamma_w \Delta z} + \frac{\gamma'}{\gamma_w} \quad (4)$$

Conversely the hydromechanical envelope for the initiation of internal instability is given by:

$$i_{\gamma cr} = \alpha \left(\frac{\sigma_{v0}}{\gamma_w \Delta z} + \frac{\gamma'}{\gamma_w} \right) \quad (5)$$

Or

$$i_{\gamma cr} = \alpha \left(\frac{\sigma_{vm}}{\gamma_w \Delta z} + \frac{\gamma'}{2\,\gamma_w} \right) \quad (6)$$

Where σ_{v0} is the vertical stress applied at the top of the specimen, or σ_{vm} is the mean vertical and Δz is the thickness of the sample over which the hydraulic gradient is measured. In these equations, the alpha factor α should not change with increasing effective stress (Shire et al 2014), however with an increased effective stress the critical hydraulic gradient will be increased. Fannin and Moffat (2006) did not supply calculated alpha factors for their tests, but here we determine these for G4-C* using Equation 5. For values of i_{cr} = 9.1 and 8, Δz =

100mm, σ_{v0} = 25 kPa, γ' ~ 10 kN/m^3 γ_w = 9.81 kN/m^3, alpha values are calculated to be α = 0.34 and 0.30, respectively.

Moffat and Fannin (2006) also describe a test using the G4-C grading but with spherical glass beads in a 460 mm length sample under downward flow and 25kPa applied top stress, with local measurement of hydraulic gradient. In this test, at the point of local failure detected within the sample, local i_{cr} = 8.7, σ_{vm} = 26.1 kPa, γ' ~ 10 kN/m^3 (estimated here) and Δz = 125mm between tapping points. This results in α = 0.4, using Equation (4).

These values are considerably lower than that calculated for G-G4-C with α = 0.6, but they also show the variability between them. Differences could be a function of variability in material shape and roughness, packing density, flow direction and stress, noting that these influences are still a subject of investigation (Shire et al., 2014, Chang and Zhang, 2013, Moffat et al., 2011), although they may also be due to random variation in particle arrangements. For example, from their DEM experiments, Shire et al. (2014) found that, for unstable materials in which the voids became filled with fines (greater than 30%) α increased as specimens increased in density, with loose samples being internally unstable and dense samples being stable. Between these extremes, there was considerable variation, even in particle systems constructed solely of spheres.

4.3 Comparison with stability criteria

Comparison of the test results can be made against the geometric stability criteria proposed by Kenney and Lau (1985), Kezdi (1979), Istomina (1957), Burenkova (1993) and Wan and Fell (2008) (modified Burenkova). We see that both Kenney and Lau (1985) and Kezdi (1979) both correctly predict the behaviour of all the tests, with GS&B-B (which restabilised after initial instability) lying most close to the instability values for the two criteria. Burenkova (1993) ascribes instability to all the tests, including GS&B-D which was stable. Istomina (1957) declares the three most unstable tests (GS&B-A, GS&B-H and G-G4-C) as

in the transition zone between stable and unstable, and the two most stable, correctly, as stable or self-filtering. The modified Burenkova assessment for gap-graded soils proposed by Wan and Fell (2008) gives instability probabilities of between 0.5 (for GS&B, which was stable) and 0.8 (for GS&B-A, which was unstable) across all tests. Although the trend appears to follow the tendency for instability correctly, the relative closeness of the determined probabilities does not inspire confidence in its use. Hence, for these tests, it appears that Kenney and Lau (1985) and Kezdi (1979) provide the best assessment of potential instability, as found also by Skempton and Brogan, Li and Fannin (2008) and Shire et al (2014).

5 IMAGE ANALYSIS

The major advantage of using transparent soil is that the particles can be visualised as 2D objects within the fluid. This in turn leads to the possibility of applying quantitative image analysis to the permeameter results. One test, GS&B-H, was carried out with additional imaging during each increment in head. As a result, this test took approximately 17 hours with typically 100 minutes between increments in head, rather than around 15 minutes as was typical for the other tests.

5.1 Void ratio

Pre test measurements showed image ‘slices’, taken at 10, 20, 30 and 40 cm depth, to have areas with open void spaces where the fines had not filled the spaces. Typically voids occurred underneath larger particles and along the glass walls of the permeameter. For the analysis to determine void ratio and subsequent changes, these colour images were converted via a thresholding technique to 8-bit greyscale. Flattening and sharpening filters were subsequently used to improve the image quality. Only the right half (50mm) of the images

was analysed in detail, due to the deteriorating image quality on the left away from the laser source (Figure 14(a)). A scale was added to each image based on immersed calibration target images taken before the test. For each image slice, the coarse fraction area and open void areas were determined by applying a mask across particular shade bands. This allowed for the darker, coarse sized particles to be preferentially highlighted, therefore allowing an area to be calculated (Figure 14(b)). A separate mask was then applied to highlight the area of 'open voids' (Figure 14(c)). Open voids are not small voids between fines, but large areas where fines are absent. These may occur in a specimen supported by coarse particles where the fines have washed out, for example. As the frame dimensions were known, the area of the coarser fraction and open voids could be subtracted from the frame area, giving an area of fine particles and 'small voids' between the particles. Using these calculated areas, parameters such as void ratio and porosity also could be determined. This analysis was carried out for the four image slices at each stage; the averaged values are presented in Table 4.

The process of choosing an intensity range to create a mask of the coarser fraction area, and the open void area, has some constraints. First, it was not possible to create a mask of the finer fraction. This was in part due to the laser sheet width, being approximately 1.5-2 mm, while particle sizes were as small as 0.4 mm. These fine particles create an intensity shade in between that of an open void and a larger particle. Second, the edges of the larger particles also have an intensity shade that is in between an open void and a solid particle, due the incidence angle at which the laser may penetrate the oblique edges of the particle. This results in an underestimate of the coarse fraction size. Third, as light becomes dissipated as it travels through the specimen, the intensity shades furthest away from the laser source are darker than those close to the laser source. As a result, the intensity shade range does not always include some void spaces at points furthest away from the laser source.

5.2 Internal erosion analysis

For the analysis of internal erosion, one image section was selected for image processing as the test progressed. The test was then split into six phases of development (arrows in Figure 13) being:

Phase 1: Beginning of test, $i_{av} = 0$.

Phase 2: When a minor movement of fines was observed along the glass edge at $i_{av} = .095$.

Phase 3: When a slight movement of fines was observed throughout the specimen (typically within open void spaces) at $i_{av} = 0.19$.

Phase 4: When a moderate amount of fines are suffusing, and small movements of the smaller of the coarse fraction occurs, at $i_{av} = 0.276$.

Phase 5: Shortly after piping initiates along the glass wall at $i_{av} = 0.35$.

Phase 6: When piping and wash out of fines is well developed, at $i_{av} = 0.48$.

The brighter half of the specimen, closest to the laser source, was divided into three sections (Figure 14(a)). Section 1 is the lower third, Section 2 the middle, and Section 3 the top. A filter to sharpen the images was also applied. Images were treated in the manner as detailed in Section 6.1.

Results are plotted in Figure 15. An analysis of this graph is given below.

- In Phases 1 and 2, Section 1 has the lowest area of open void space, while Section 3 has the highest. This may be due to more fine particles falling into the lower section or greater compaction in the lower section to begin with.
- By Phase 3, Section 1 has an increased volume of open voids, while Section 2 has a decreased volume. This shows fines moving out of Section 1, and into Section 2. Section 3 also has an increasing open void volume, showing it too is losing fines.

– Phase 4 shows the trend in Phase 3 developing further. Section 2 continues to gain fines, while Sections 1 and 3 lose fines.
– Phase 4 shows a break in trend for Section 2, where it begins a slight net gain in open void space (net loss of fines). Sections 1 and 3 shows an accelerated increase in open void volume.
– In Phase 5, the initiation of piping results in a large net loss in fines in Section 2 at a greater rate than Sections 1 and 3. This occurs due to the fact that Section 2 has more fines to lose at this point.

At the end of the test in Phase 6, all three zones finish with a similar amount of open void space volume, with Section 1 having the least volume and Section 3 having the greatest amount of open void volume. Section 1 showed an increase of four times, Section 2 showed a 2.7-fold increase, and Section 3 had a two-fold increase in open void space.

In this analysis, the use of thresholding techniques on images obtained from PLIF during a test enabled coarse fractions, areas of open void space and areas of fines to be distinguished. The results show that, although precisely determined quantities of fine and coarse fractions were not obtained, by using relative quantitative analysis of the images taken at discrete locations during key phases of a test, additional insight to the internal erosion process was obtained. Specifically, the local fines movement from the bottom of the sample through to the top was seen to initiate before significant change in the local hydraulic gradient (e.g. between Phases 2 and 3) was manifested (compare Figures 14 and 16).

6 CONCLUSIONS

Experiments using a new rigid walled permeameter show that test materials fabricated from irregular particles of optically matched glass and oil match well the typical behaviour of soil

and water under seepage flow conditions. Results are validated against published data on both coarse and fines supported soil samples under upward flow, showing very good agreement for both internally unstable and stable materials. Images taken of an illuminated plane within specimens during testing provide further insight into how fines are distributed within a sample before testing and while seepage flow is applied. It is seen that in internally unstable materials, local movement of fine particles progress from "dancing" within voids under low hydraulic gradients to migration between the larger clasts at larger hydraulic gradients. Quantitative image analysis shows fabric rearrangement beginning to occur just before local changes in permeability is detected at the side walls and that continued change is directly linked to fines migration.

Common methods to characterize the susceptibility of a sample to internally erode were applied to the particle size distributions before testing. Results show that the criteria proposed by Kenney and Lau (1985, 1986) and Kezdi (1979) provide good guidance as to the propensity for a material to erode internally. Coupled with an understanding of the dominant load-carrying fabric, this may enable bulk behaviour to be predicted under critical seepage flow.

Images and image sequences further show how – in an internally unstable material under seepage flow – fabrics that are dominated by coarse particles exhibit suffusion under critical seepage with little evident settlement, despite piping induced local erosion of fines; while in fabrics in which loads are supported by both coarse and fine particles, fines migration via pipe formation can lead to void growth followed by structure collapse, volume change and settlement – i.e. suffosion .

ACKNOWLEDGEMENTS

The authors would like to thank the New Zealand Society on Large Dams (NZSOLD) for financial support of this project, and to acknowledge the assistance of technicians at the University of Canterbury, New Zealand in the design and construction of the apparatus.

REFERENCES

Burenkova, V. V. (1993) Assessment of suffosion in non-cohesive and graded soils In Filters in Geotechnical and Hydraulic Engineering. (Brauns, Helbaum, andSchuler (eds)) Balkema, Rotterdam, pp. 357-360.

Chang, D. S. & Zhang, L. M. (2013) Critical hydraulic gradients of internal erosion under complex stress states. Journal of Geotechnical and Geoenvironmental Engineering **139**:1454-1467.

Fannin, R. J. & Moffat, R. (2006) Observations on internal stability of cohesionless soils. Géotechnique **56(7)**:497-500.

Fannin, R. J. & Slangen, P. (2014) On the distinct phenomena of suffusion and suffosion. Géotechnique Letters **4**: 289-294.

Hunter, R. P. (2012) Development of transparent soil testing using planar laser induced fluorescence in the study of internal erosion of filters in embankment dams. MSc Thesis, University of Canterbury, New Zealand.

Istomina, V. S. (1957) Filtration Stability of Soils (in Russian). Moscow, Leningrad, Gostroizdat.

Kenney, T. C. & Lau, D. (1985) Internal stability of granular filters. Canadian Geotechnical Journal **22**:215-225.

Kezdi, A. (1979) Soil Physics - Selected Topics. Amsterdam, Elsevier Scientific Publishing Co.

Li, M. (2008) Internal instability in widely graded soils. PhD Thesis, University of British Columbia, Canada.

Li, M. and Fannin, R.J. (2008) Comparison of two crietria for internal stability of granular soil. Canadian Geotechnical Journal **45**: 1303–1309

Li, M. & Fannin, R. J. (2012) A theoretical envelope for internal instability of cohesionless soil. Geotechnique **62(1)**:77-80.

Marot, D., Bendahmane, F. & Nguyen, H.H. (2012) Influence of angularity of coarse fraction grains on internal erosion process La Houille Blanche **6**: 47-53

Matsushima, T. Ishii, T. & Konagai, K. (2002) Observation of grain motion in the interior of a PSC test specimen by laser-aided tomography, Soils and Foundations **42**(5), 27-56.

Moffat, R. & Fannin, R. J. (2006) A large permeameter for study of internal stability in cohesionless soils. Geotechnical Testing Journal 29(4): GTJ100021.

Moffat, R., Fannin, R. J. & Garner, S. J. (2011) Spatial and temporal progression of internal erosion in cohesionless soil. Canadian Geotechnical Journal **48**:399-412.

Ouyang, M. & Takahashi, A. (2015) Optical quantification of suffosion in plane strain physical models. Geotechnique Letters **5**:118–122.

Rosenbrand, E. & Dijkstra, J. (2012) Application of image subtraction data to quantify suffusion. Geotechnique Letters**(2)**:37-41.

Sanvitale, N. & Bowman, E. T. (2012) Internal imaging of saturated free surface flows. International Journal of Physical Modelling in Geotechnics **12(4)**:129-142.

Shire, T., O'Sullivan, C., Hanley, K. J. & Fannin, R. J. (2014) Fabric and effective stress distribution in internally unstable soils. Journal of Geotechnical and Geoenvironmental Engineering:04014072.

Skempton, A. W. & Brogan, J. M. (1994) Experiments on piping in sandy gravels. Géotechnique **44(3)**:449-460.

Terzaghi, K. (1925) Erdbaumechanik. Vienna, Deuticke.

Wan, C. F. & Fell, R. (2008) Assessing the potential of internal instability and suffusion in embankment dams and their foundations. Journal of Geotechnical and Geoenvironmental Engineering **134(3)**:401-407.

TABLES

Table 1. Physical and optical properties of the materials at 25° C

	Refractive index at 589.3nm	Density (kg/m^3)	Kinematic viscosity (mm^2/s)
Immersion oil	1.472	846	16
Duran glass	1.475	2230	-

Table 2. Stability criteria applied to mixtures tested.

Stability Criterion	**Key quantity**	**GS&B-A**	**GS&B-B**	**GS&B-D**	**G-G4-C**	**GS&B-H**
Kenney & Lau (1985)	$(H/F)_{min}$	0 (unstable)	0.86 (just unstable)	3.57 (stable)	0 (unstable)	0.27 (unstable)
Kezdi (1979)	(D'_{15}/d'_{85}) @ $(H/F)_{min}$	8.9 (unstable)	4.3 (just unstable)	3.6 (stable)	6.5 (unstable)	7.2 (unstable)
Istomina (1957)	$C_u = (D_{60}/D_{10})$	19.13 (transition)	8.05 (self filtering)	4.03 (self filtering)	11.67 (transition)	15.3 (transition)
Burenkova (1993)	h' and h''	Unstable	Unstable	Unstable	Unstable	Unstable
Modified Burenkova	Probability, P	0.80	0.60	0.50	0.75	0.65
	Porosity n	0.27	0.29	0.29	0.266	0.282
Stable hydraulic gradient	i_c	1.194	1.162	1.162	1.201	1.175
Hydraulic gradient observed	i_{cr}	0.248	0.300 or 1.014*	1.13	0.72	0.15
Alpha factor i_{cr}/ i_c	α	0.208	0.258 or 0.849*	0.973	0.600	0.128
Notes on stability	Kenney & Lau (1985): $(H/F)_{min} < 1$ (unstable) Kezdi (1979): $(D'_{15}/d'_{85})_{max} > 4$ (unstable); Istomina (1957): $C_u = (D_{60}/D_{10}) < 10$ (self-filtering or stable), >20 (unstable) Modified Burenkova after Wan & Fell (2008): Probability of internal instability, P Stable hydraulic gradient for heave after Terzaghi (1925) * Two values are given as material restablised after initiation of internal instability until heave occurred.					

Table 3. Comparison of results from current test series using glass-oil mixtures and equivalent tests in the literature. Data for comparison from Skempton and Brogan (1994) and Fannin and Moffat (2006).

Glass – oil tests	**GS&B-A**	**GS&B-B**	**GS&B-D**	**G-G4-C**	**GS&B-H**
n	0.27	0.27	0.29	0.266	0.282
$k_{initial}$ (cm/s)	0.30	1.00	0.18	0.02	0.50
i_c	1.19	1.16	1.16	1.20	1.175
i_{cr}	0.25	0.300 / 1.01	1.31	0.72	0.15
α	0.21	0.26 / 0.85	1.13	0.60	0.13
Failure mode	Piping	Piping / heave	Heave	Piping with suffusion / volume change	Piping
Soil - water tests	**S&B-A**	**S&B-B**	**S&B-D**	**G4-C***	**N/A**
n	0.34	0.37	0.365	0.24	-
$k_{initial}$ (cm/s)	0.45	0.84	1.80	0.022	-
i_c or $i_{\gamma c}$	1.09	1.04	1.05	53	-
i_{cr} or $i_{\gamma cr}$	0.20	0.34	1.0	9.1, 8.0	-
α	0.18	0.33	0.95	0.34, 0.30	-
Failure mode	Piping	Piping	Heave	Piping with suffusion / volume change	-

Table 4 Calculated parameters from image processing of GS&B-H

	Averages	
	Pre-test	Post-test
Frame Area, Vt (mm^2)	5829	5861
Coarse Fraction Area, Vc (mm^2)	3175	2920
Open Void Area, Vv (mm^2)	674	1108
Fine Fraction + small void Area: Vt - Vc - Vv (mm^2)	1980	1832
Total Solid Area + small voids: Vt – Vv (mm^2)	5155	4752
Coarse Fraction Open Void Ratio: Vv/Vc	0.215	0.368
Open Void Ratio, e_o : Vv / (Vt – Vv)	0.131	0.233
Sample Void Ratio, e	0.392	0.392
Open void Porosity, n_o :Vv / Vt	0.116	0.189
Sample Porosity, n	0.282	0.282
Porosity of Fine Fraction, n_f : $n - n_o$	0.166	0.093

FIGURE CAPTIONS

Figure 1: Permeameter dimensions, manometer ports denoted p1 to p5.

Figure 2: Image of apparatus set up including, clockwise from top left: header tank, manometers, permeameter illuminated by laser sheet, and camera.

Figure 3: Particle size distributions for materials tested (blue) against equivalents of Skempton and Brogan (1994) and Fannin and Moffat (2006) (black). Note grain size scaling of 4 applied to GS&B-A GS&B-B and GF&M G4-C, and a factor 2 to GS&B-D.

Figure 4: Pre test images of sample GS&B-A at a) 10 mm; b) 20 mm and; c) 30 mm from front of apparatus.

Figure 5: Test GS&B-A: hydraulic gradient against flow velocity

Figure 6: Test GS&B-A Before test and at an average hydraulic gradient i_{av} = 0.38

Figure 7: Test GS&B-B: hydraulic gradient against flow velocity

Figure 8: GS&B-B indicative changes in microstructure at increasing hydraulic gradient: i_{av} = 0.10 to i_{av} = 0.16 (minor changes circles in white); i_{av} = 0.23 to i_{av} = 0.50 (more major change in white); i_{av} = 0.621 to i_{av} =1.014 when the sample failed by 'heave'. Note air bubbles in oil degrading image quality at i_{av} = 0.621 and gap in material for i_{av} = 1.014 where upper portion of sample has heaved.

Figure 9: Test GS&B-D: hydraulic gradient against flow velocity

Figure 10: Test GS&B-D: Before test and after failure by heave.

Figure 11: Average hydraulic gradient vs. flow velocity for test GF&M-G4C.

Figure 12: GF&M-G4C at (a) i_{av} = 0 and (b) i_{av} = 0.72. Note the changes in clast (large particle structure) due to suffusion.

Figure 13 Average hydraulic gradient vs. flow velocity for test GS&B-H. Also showing 6 phases of movement.

Figure 14 An example of 'masks' created from a) an unprocessed image, to highlight; b) the coarser fraction (in white), and; c) open void space (in white).

Figure 15 Image analysis results of open void space with phases of movement.

SUPPLEMENTARY VIDEOS

S1 – Sample test GS&B-A2: Small pipe formation – suffusive behaviour

S2 – Sample test GF&M-G4C: Failure – suffosive behaviour

Hunter & Bowman

Figures

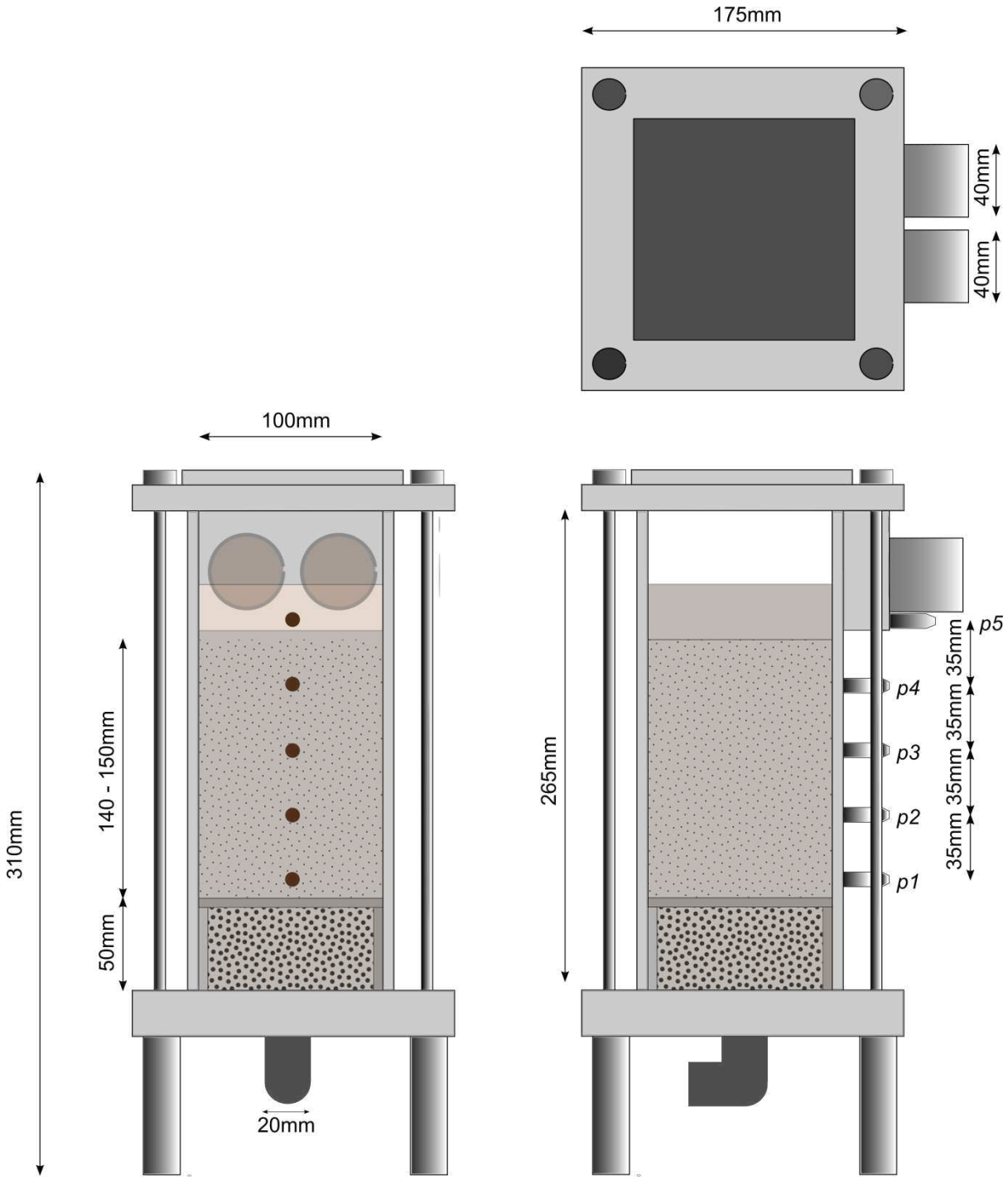

Figure 1: Permeameter dimensions, manometer ports denoted p1 to p5.

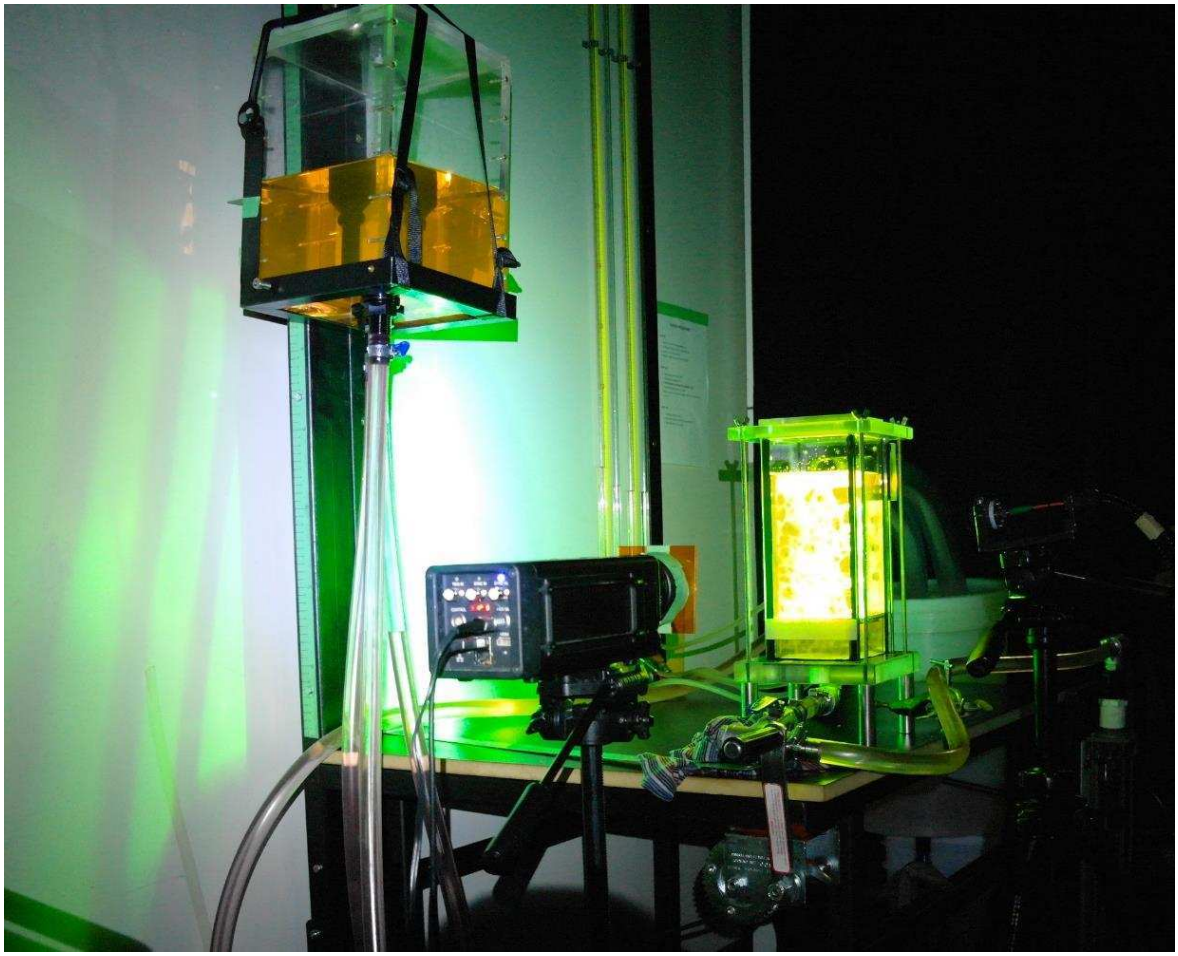

Figure 2: Image of apparatus set up including, clockwise from top left: header tank, manometers, permeameter illuminated by laser sheet, and camera.

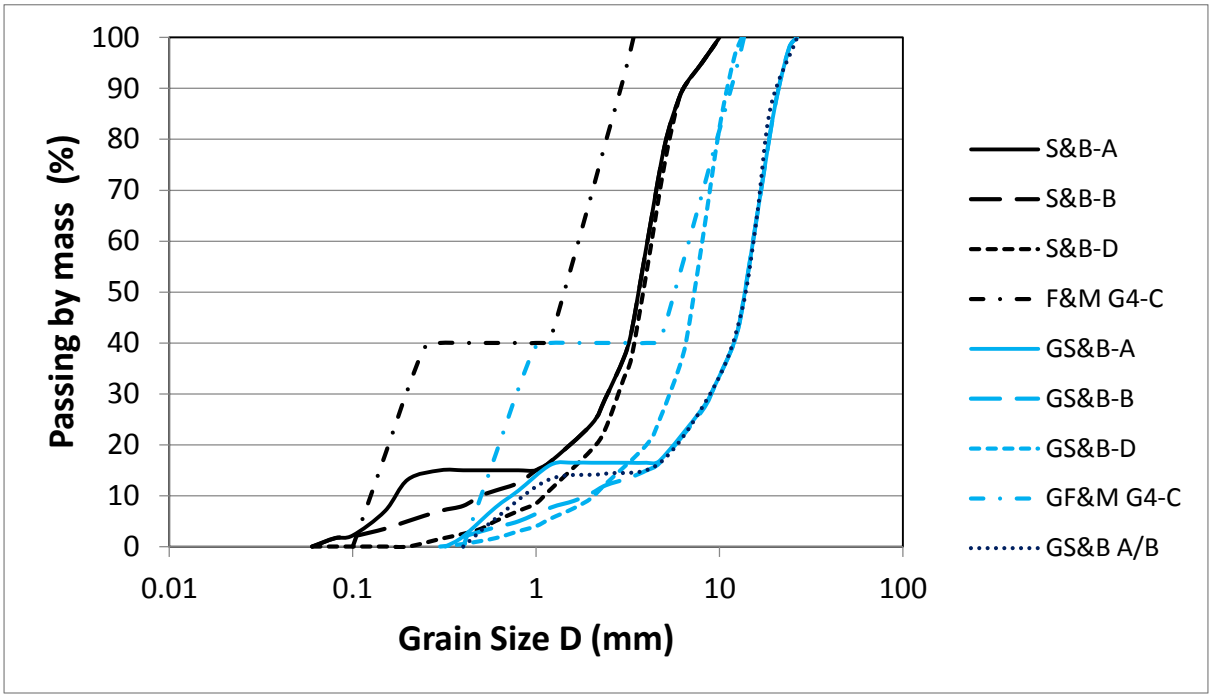

Figure 3: Particle size distributions for materials tested (blue) against equivalents of Skempton and Brogan (1994) and Fannin and Moffat (2006) (black). Note grain size scaling of 4 applied to GS&B-A GS&B-B and GF&M G4-C, and a factor 2 to GS&B-D.

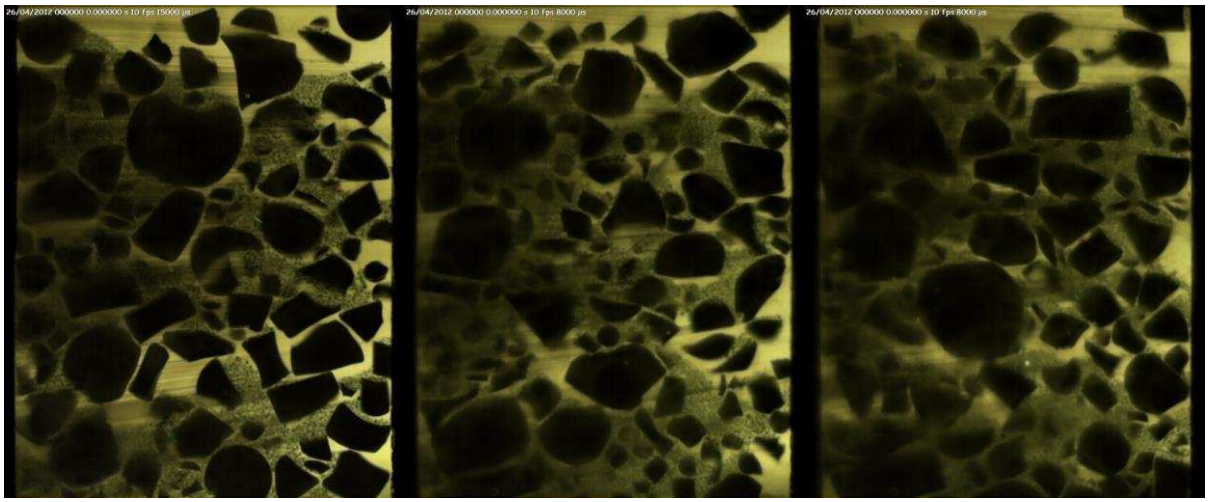

Figure 4: Pre test images of sample GS&B-A at a) 10 mm; b) 20 mm and; c) 30 mm from front of apparatus.

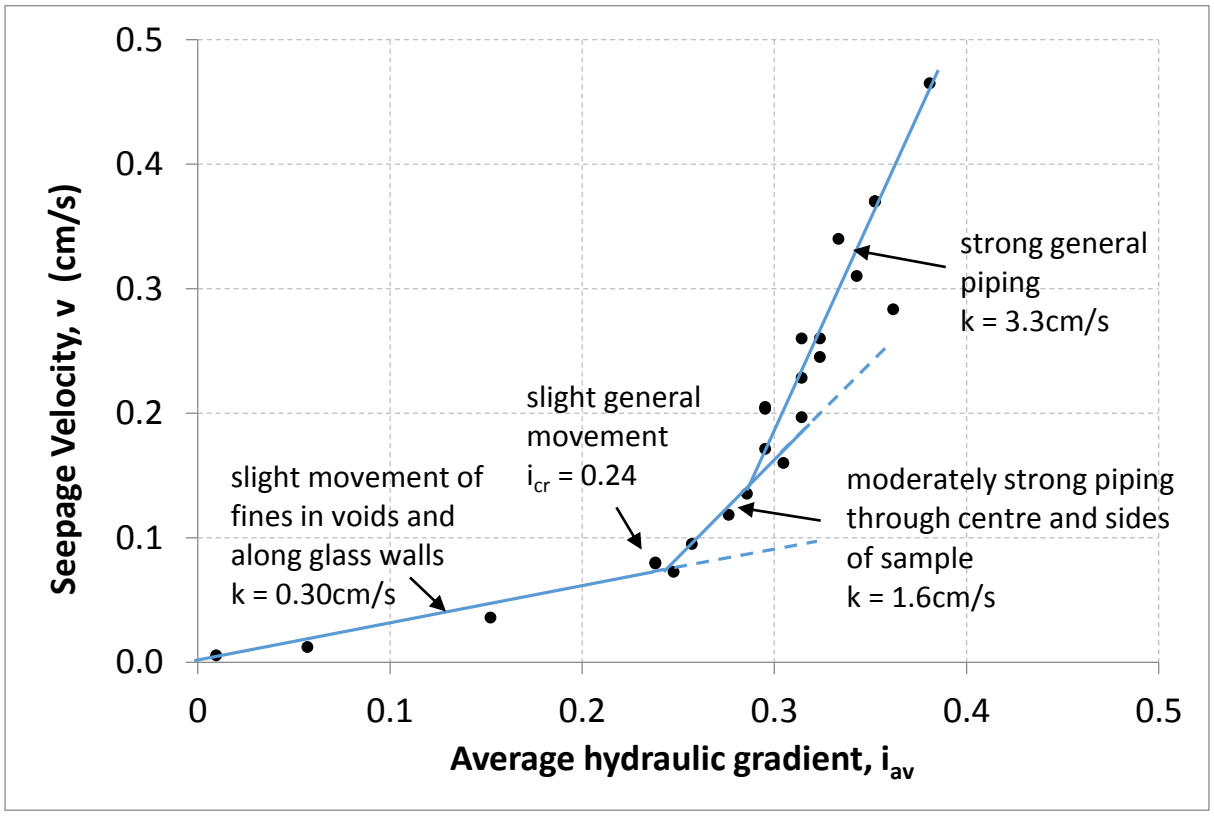

Figure 5: Test GS&B-A: hydraulic gradient against flow velocity

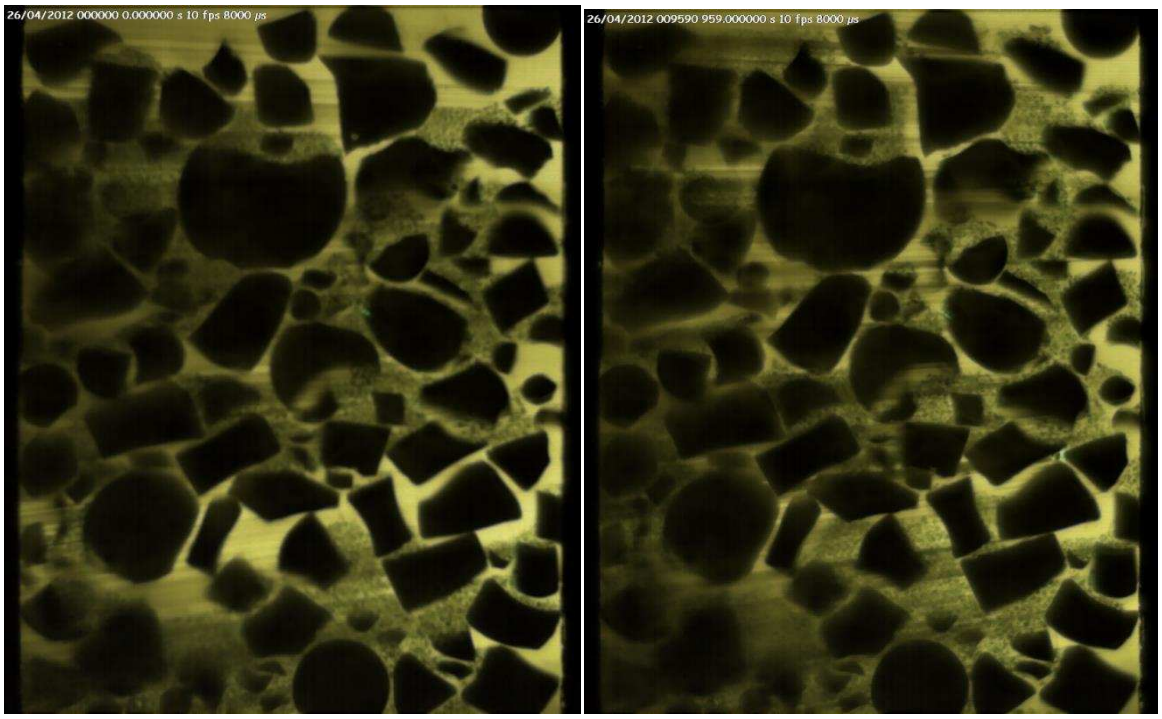

Figure 6: Test GS&B-A Before test and at an average hydraulic gradient i_{av} = 0.38

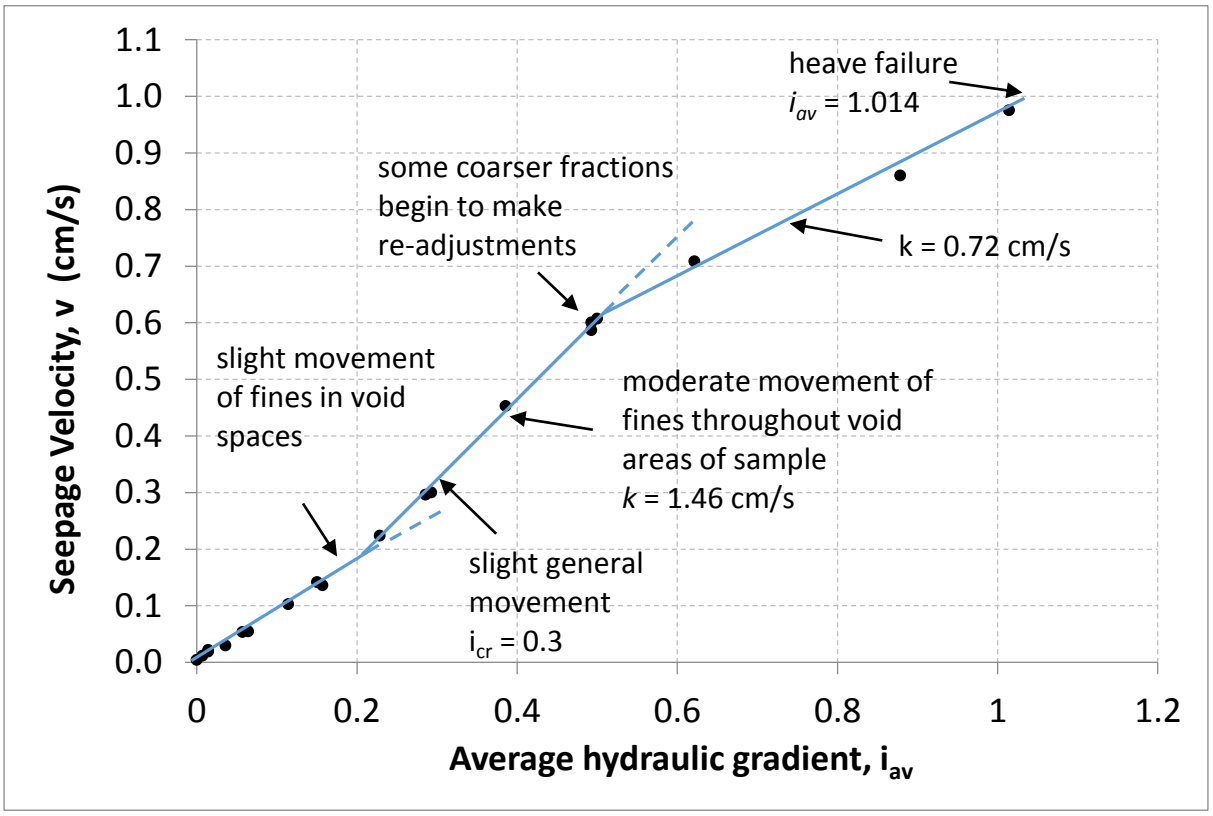

Figure 7: Test GS&B-B: hydraulic gradient against flow velocity

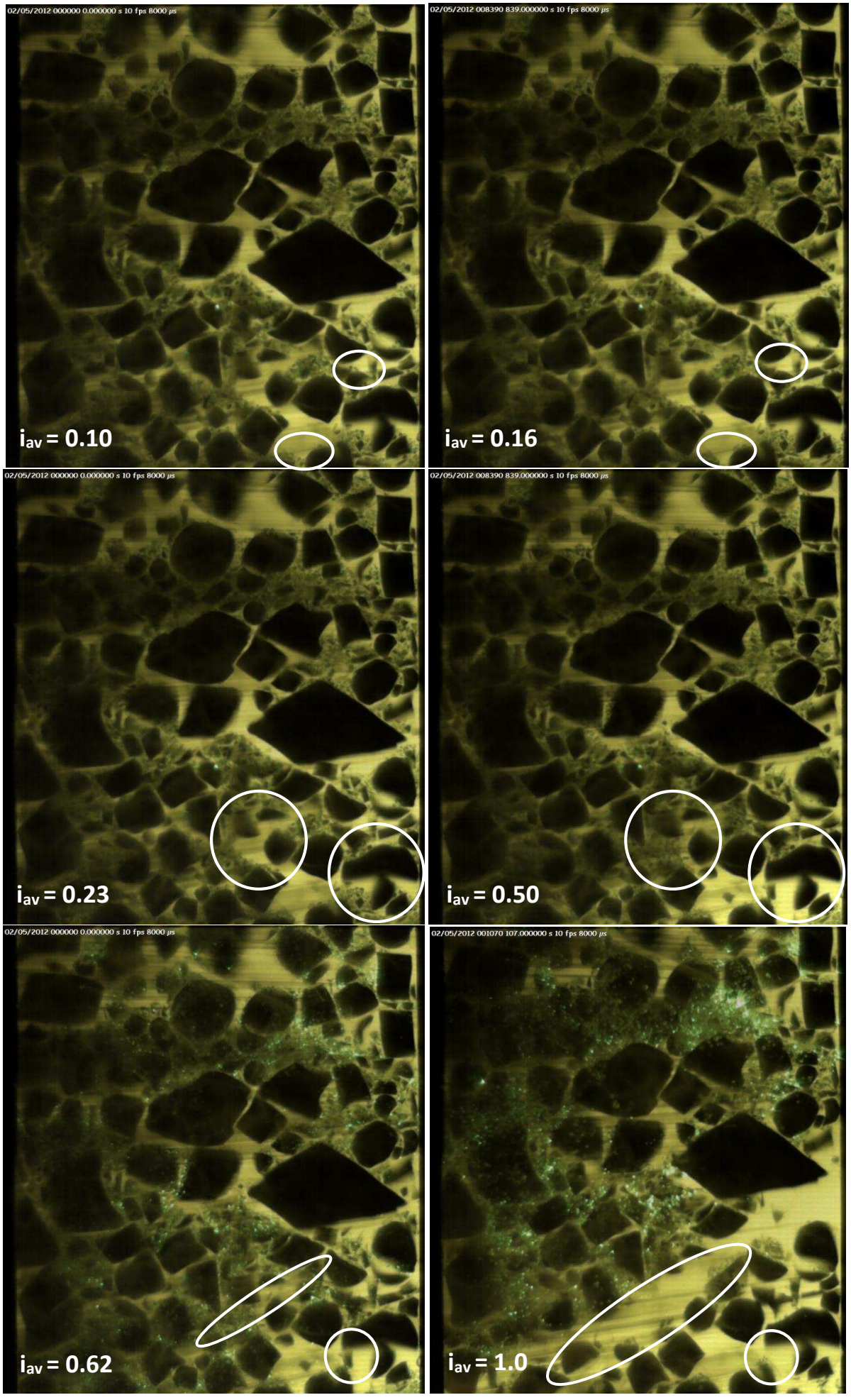

Figure 8: GS&B-B indicative changes in microstructure at increasing hydraulic gradient: i_{av} = 0.10 to i_{av} = 0.16 (minor changes circles in white); i_{av} = 0.23 to i_{av} = 0.50 (more major change in white); i_{av} = 0.621 to i_{av} =1.014 when the sample failed by 'heave'. Note air bubbles in oil degrading image quality at i_{av} = 0.621 and gap in material for i_{av} = 1.014 where upper portion of sample has heaved.

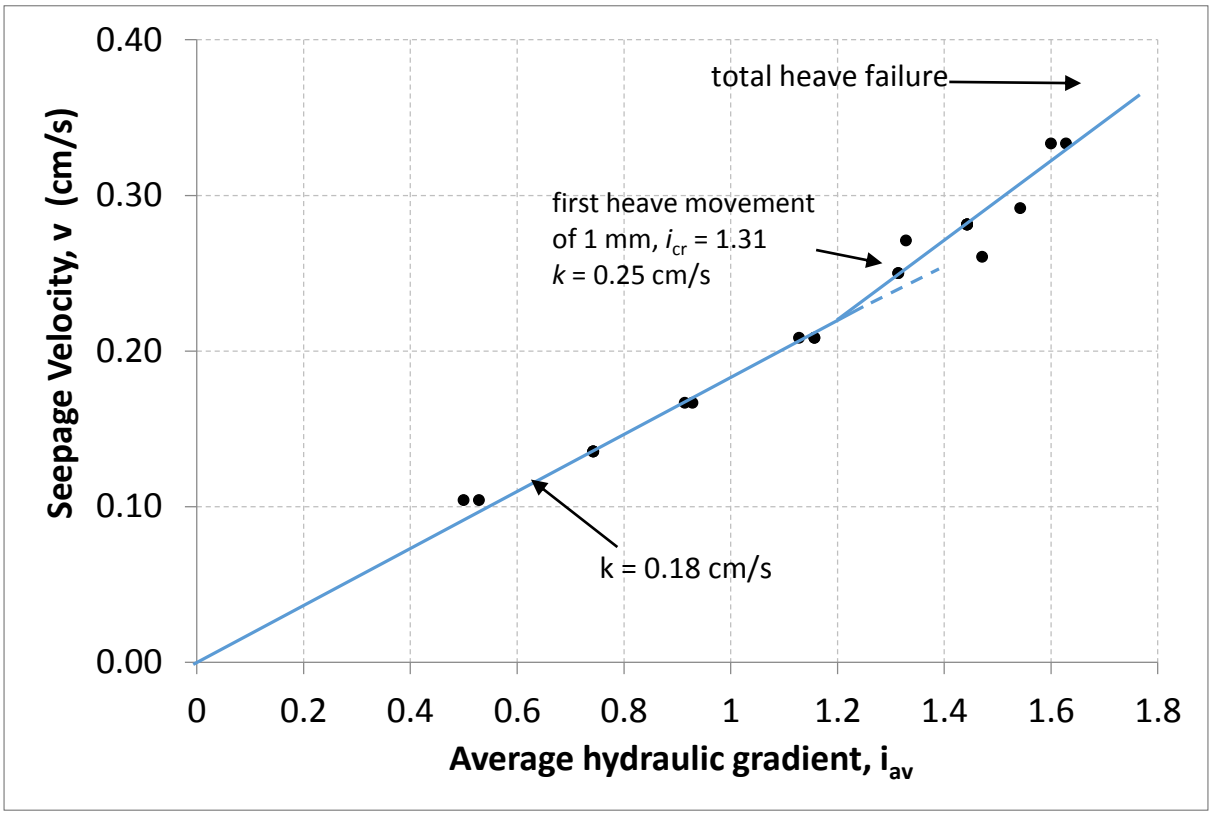

Figure 9: Test GS&B-D: hydraulic gradient against flow velocity

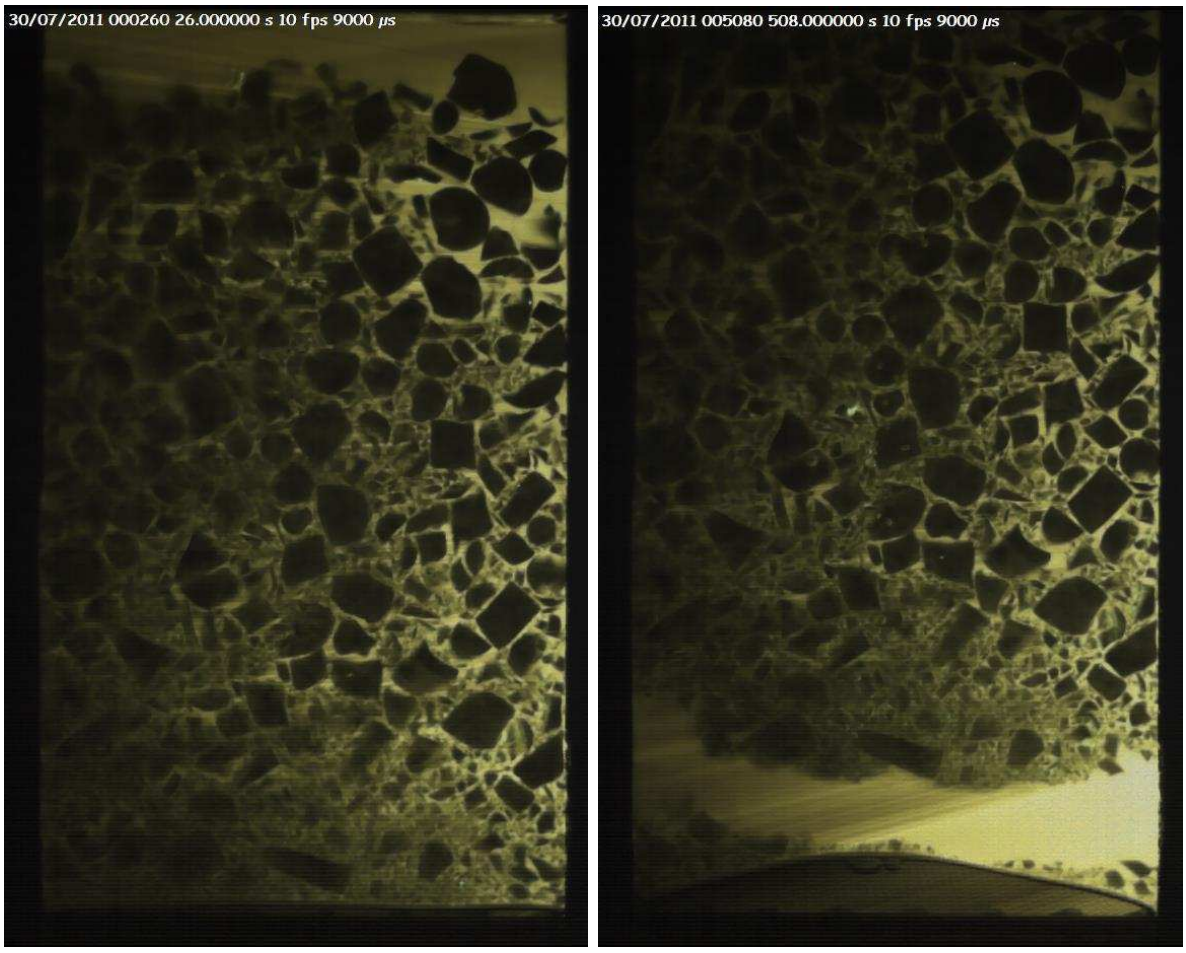

Figure 10: Test GS&B-D: Before test and after failure by heave.

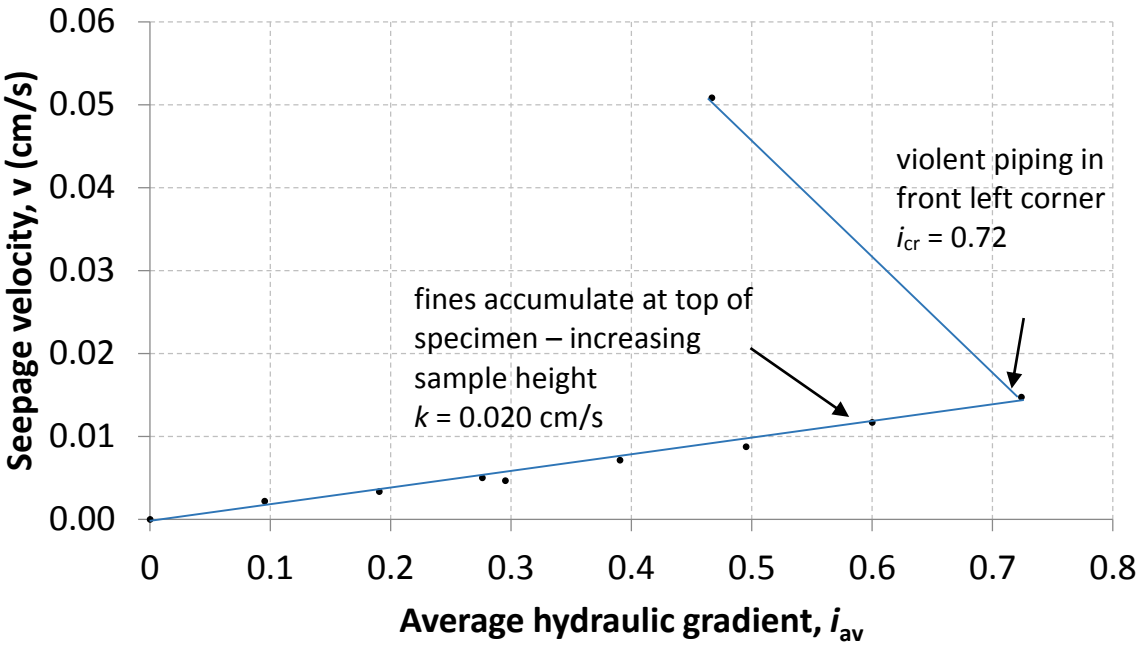

Figure 11: Average hydraulic gradient vs. flow velocity for test GF&M-G4C.

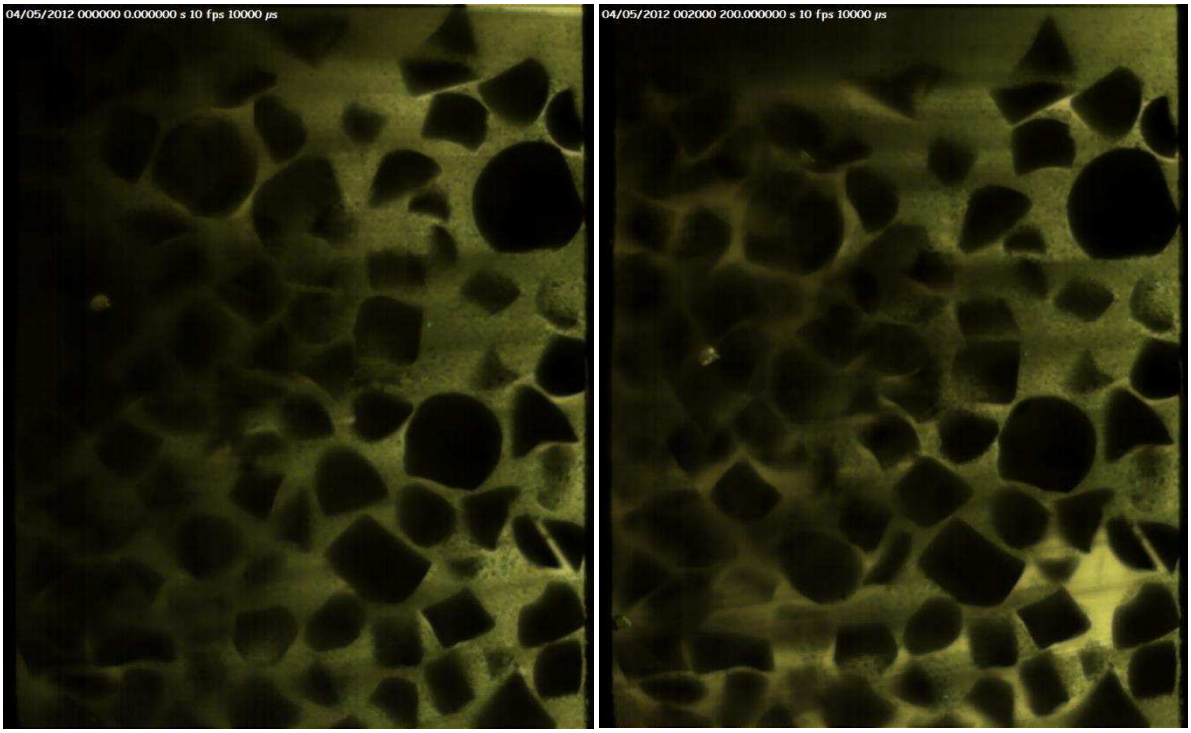

Figure 12: GF&M-G4C at (a) i_{av} = 0 and (b) i_{av} = 0.72. Note the changes in clast (large particle structure) due to suffusion.

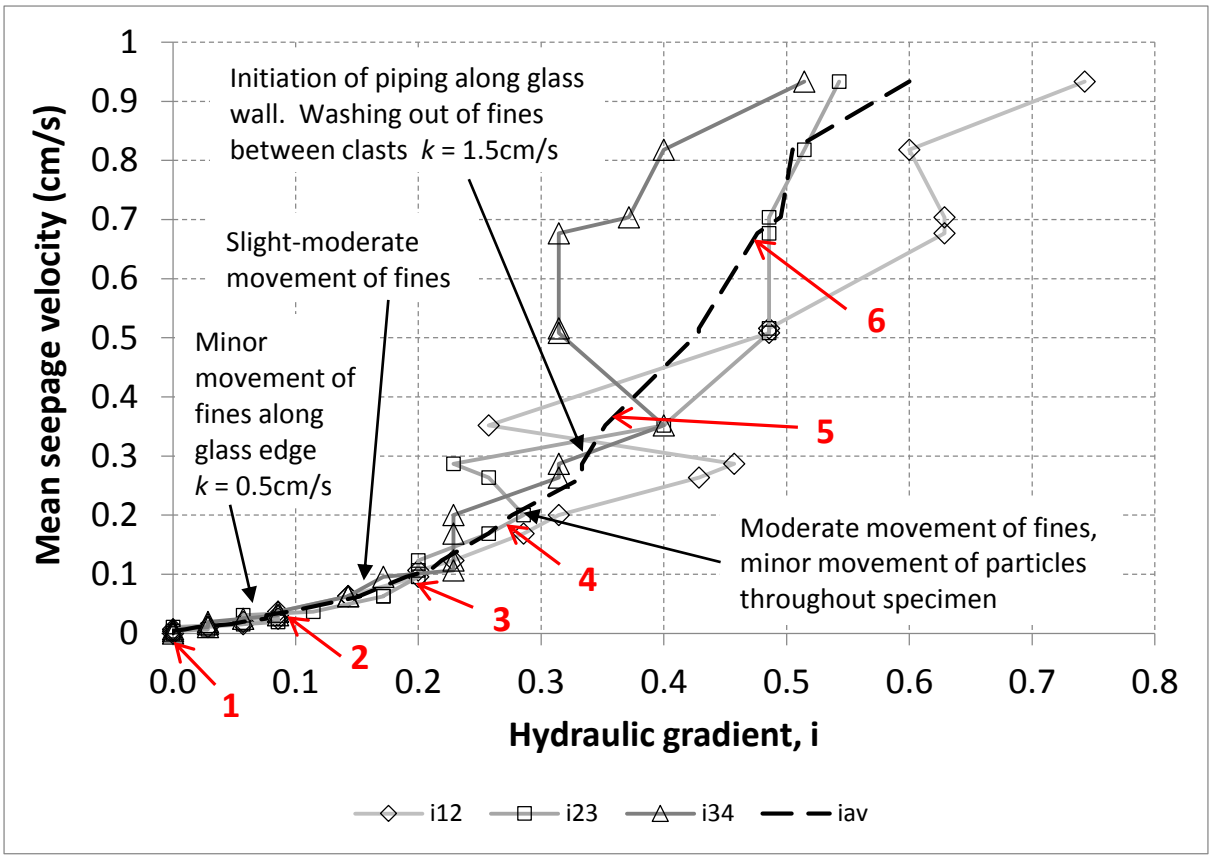

Figure 13 Average hydraulic gradient vs. flow velocity for test GS&B-H. Also showing 6 phases of movement.

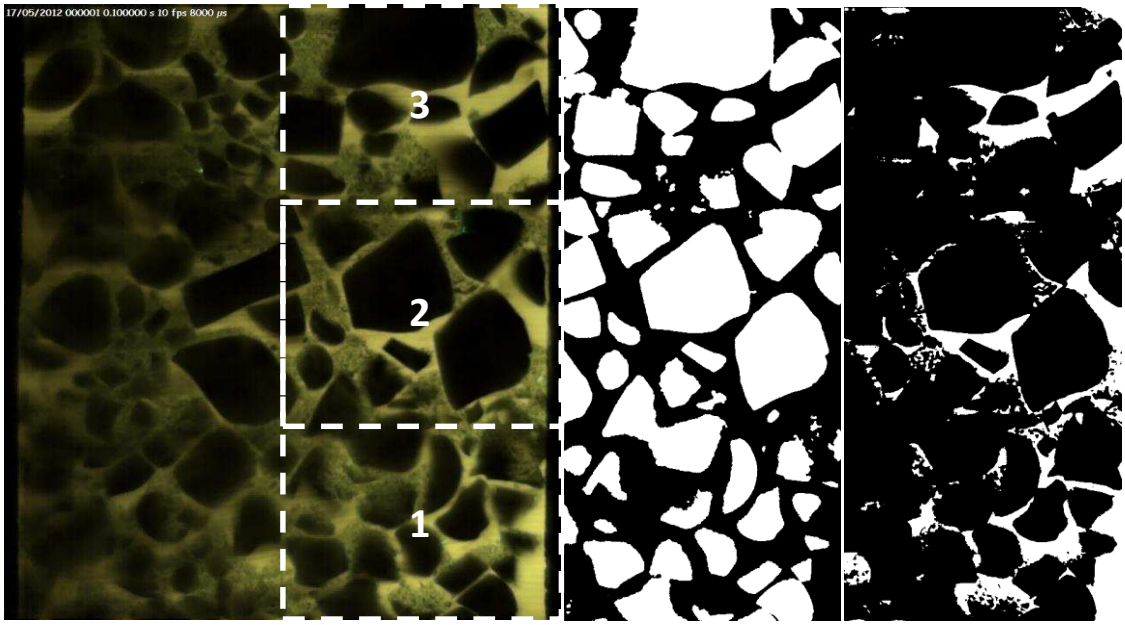

(a) (b) (c)

Figure 14 An example of ‘masks’ created from a) an unprocessed image, to highlight; b) the coarser fraction (in white), and; c) open void space (in white).

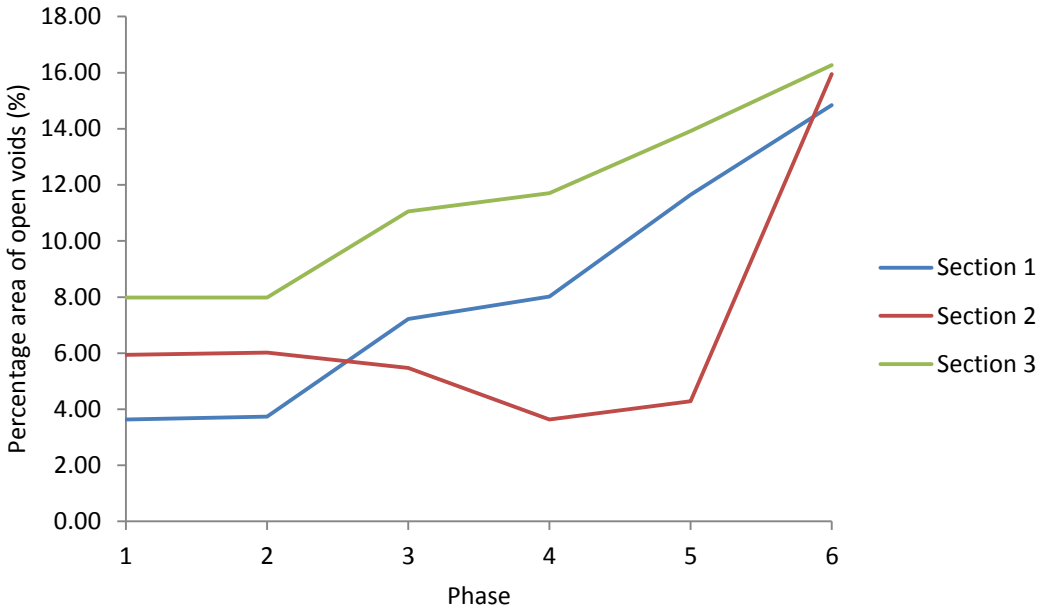

Figure 15 Image analysis results of open void space with phases of movement.

Journal Publishing Agreement

It is our policy to ask authors to assign the copyright of articles accepted for publication to the Publisher. Exceptions are possible for reasons of national rules or funding. Please tick the relevant options below.

In assigning copyright to us, you retain all proprietary rights including patent rights, and the right to make personal (non-commercial) use of the article, subject to acknowledgement of the journal as the original source of publication.

By signing this agreement, you are confirming that you have obtained permission from any co-authors and advised them of this copyright transfer. Kindly note that copyright transfer is not applicable to authors who are opting to publish their papers as Open Access. Open Access authors retain copyright of their published paper.

Please complete the form below and return an electronic copy to your ICE Publishing contact: (http://www.icevirtuallibrary.com/info/submit).

Journal name: Geotechnique

Article title: Visualisation of seepage induced suffusion and suffosion within internally erodible granular media

Manuscript reference number: 17-P-161

Authors: Robert P Hunter and Elisabeth T Bowman

Your name: Elisabeth T Bowman

Signature and date: 1st Nov 2017

Please tick either one option from part A or one option from part B. Please complete part C.

A. Copyright

☐ I hereby assign and transfer the copyright of this paper to Thomas Telford Ltd.

☐ British Crown Copyright: I hereby assign a non-exclusive licence to publish to Thomas Telford Ltd.

☐ I am a US Government employee: employed by (name of agency) ……

☐ I am subject to the national rules of (country) …… and confirm that I meet their requirements for copyright transfer or reproduction (please delete as appropriate)

B. Authors with open access funding requirements. Please specify the Creative Commons license version required.

☐ CC-BY (for full details click here Creative Commons Attribution (CC BY) 4.0 International License)

☒ CC-BY-NC-ND (for full details click here Creative Commons Attribution Non Commercial No-derivatives (CC BY NC ND) 4.0 International License)

C. Please confirm that you have obtained permission from the original copyright holder. For ICE Publishing's copyright policy, please click here. ICE Publishing is a signatory to the STM Guidelines.

☒ I have obtained permission from the original copyright holder for the use of all subsidiary material included in this paper (E.g. for borrowed figures or tables).